An atomistic study on grain-size and temperature effects on mechanical properties of polycrystal CoCrFeNi high-entropy alloys

Lu Xie [a],[1], Guangda Wu [a],[1], Qing Peng [b],[d],[*], Junpeng Liu [c], Dongyue Li [a], Wenrui Wang [a],[**]

[a] School of Mechanical Engineering, University of Science and Technology Beijing, Beijing 100083, China
[b] State Key Laboratory of Nonlinear Mechanics, Institute of Mechanics, Chinese Academy of Sciences, Beijing 100190, China
[c] Key Laboratory of Advanced Materials of Ministry of Education, School of Materials Science and Engineering, Tsinghua University, Beijing 10084, China
[d] School of Engineering Sciences, University of Chinese Academy of Sciences, Beijing 100049, China

ARTICLE INFO

ABSTRACT

The origin of the outstanding mechanical properties of high-entropy alloys (HEAs) is still elusive. In this paper, we have investigated the influence of grain size and temperature on the mechanical properties of polycrystalline CoCrFeNi HEAs via molecular dynamics simulations. The critical grain size for the inverse Hall-Petch effect in CoCrFeNi HEAs is approximately 11.65 nm. During the stage of the positive Hall-Petch effect (where smaller grain sizes lead to higher tensile strength), there is a positive correlation between the tensile strength and dislocation density in CoCrFeNi HEAs. The higher tensile strength at low temperatures in CoCrFeNi HEAs is also attributed to an increase in dislocation density. At low temperatures, the reduced thermal vibrations of atoms slow down the motion of dislocations, leading to an increased storage time of dislocations within the crystal. In the stage of the inverse Hall-Petch effect, due to a significant reduction in grain size, the storage capacity of dislocations within grains decreases. This leads to the accumulation of more dislocations at grain boundaries, forming defects, and consequently causing a decrease in the tensile strength of CoCrFeNi HEAs as the grain size decreases. Our results might be helpful in material design of polycrystal HEAs.

1. Introduction

High-entropy alloys are multi-principal elements alloys based on equi-atomic or near-equi-atomic mixtures of five or more elements [1, 2]. Due to the unique compositions and structures, HEAs demonstrate remarkable characteristics, including superior strength, exceptional hardness, excellent resistance to wear, high corrosion resistance, and good high-temperature stability [3–9]. HEAs become a hot research topic in materials science and engineering, especially due to their excellent mechanical strengths. However, the origin of HEAs strength is still elusive and desirable for further investigation [10].

The mechanical properties of HEAs vary with temperatures [11–13]. It is interesting that HEAs have higher yield strength and tensile strength at low temperatures (<273 K) while maintaining good ductility and fracture toughness [14]. Li et al. [15] investigated the mechanical characteristics of $Al_{0.1}CoCrFeNi$ and $Al_{0.3}CoCrFeNi$ at various temperatures and found that decreasing temperature enhances their strength

and elongation. Liu et al. [16] investigated the strength and ductility of CoCrFeNi at low temperatures and found that at 4.2 K, the tensile strength of the alloy reached 1251 ± 10 MPa, and the failure strain reached 62 %. Twinning is promoted at low temperatures due to the low stacking fault (SF) energy [17]. The microstructure of HEAs contains multiple equi-atomic elements, which allows the formation of a homogeneous solid solution structure at low temperatures [18]. This can be advantageous in impeding the motion of dislocations and twinning, ultimately enhancing both the strength and ductility of the material. At room temperature, the strength and ductility of HEAs also remain at a high level [19]. This is because the microstructure of HEAs at room temperature contains multiple lattice mismatches and structural irregularities, which hinder dislocation slip and enhance the tensile strength of the material. Additionally, the crystal orientation in HEAs also has a significant impact on the plastic deformation [20,21]. At non-low temperatures (> 273 K), the strength and ductility of HEAs have the trend of decreasing gradually. The yield strength and tensile strength decrease
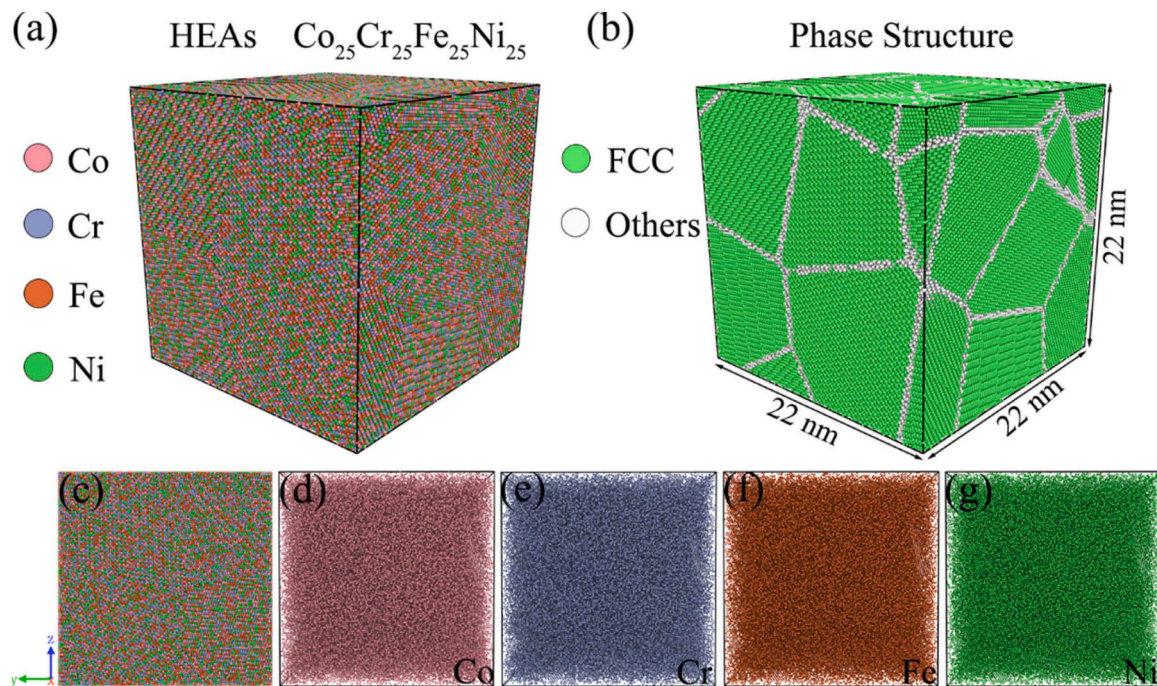

Fig. 1. The model of polycrystal CoCrFeNi HEAs in Face-Centered Cube phase. The pink, light-blue, orange, and green balls stand for the Co, Cr, Fe, and Ni atoms, respectively. (a) Tilt-view of the whole simulation box and (b) with grain boundaries. (c) Sideview of the whole box. Sideview of the distributions of (d) Co, (e) Cr, (f) Fe and (g) Ni elements.

with increasing temperature, and the ability of plastic deformation also gradually decreases [22]. High temperatures promote phase transition (PT) in HEAs, such as the transformation from a face-centred cubic (FCC) structure to a body-centred cubic (BCC) structure, which decreases the ability of plastic deformation of the material [23].

The grain size has a considerable impact on the material strength [24,25]. The Hall—Petch effect (smaller is stronger) is a frequently observed occurrence in materials with a coarse-grained structure [26–28]. However, some researchers have found the inverse Hall—Petch effect in materials with nanocrystalline grains [29–31], in which the material strength decreases as the grain size decreases below a critical value. This critical value of grain size depends on material compositions, and it is typically at the nanometre scale. Hu et al. [32] found that the strength of nano Ni-Mo material becomes softer when the grain size is approximately 10 nm. The preparation of materials with nanoscale grain sizes in experiment has considerable technique difficulties. Comparatively, computational simulations are suitable to investigate the grain size effect in nanometres. Molecular dynamics (MD) simulation is a well-established approach for the study of nanoscale deformation processes of materials [33–41]. Pan et al. [33] employed MD simulations to investigate the strength of entropy-stabilized alloys in polycrystalline $Fe_{80-x}Mn_xCo_{10}Cr_{10}$ correlating with the grain sizes. They found that the inverse Hall—Petch effect occurred at a critical grain size of 11.9 nm.

In addition to grain boundaries, lattice defects such as dislocations and twinning are also important factors affecting the mechanical characteristics of HEAs [42–46]. Dislocations are defects in the crystal structure that result from deformation of the atomic arrangement in the lattice, and they affect the strength and plasticity of HEAs [47]. The dislocation activity path and propagation mode in HEAs are different from those in traditional single-component metals. Dislocations in HEAs tend to move in multiple crystal directions rather than in a single crystal direction [48]. The particular arrangement of dislocations can enhance the strength of HEAs without compromising their ductility. Dislocations in HEAs are often subject to bend and twist due to the influence of other lattice defects [21]. Dislocations interact with other crystal defects, such

as twinning and phase boundaries, affecting the mechanical characteristics of the materials [49]. The interaction between dislocations and grain boundaries (GBs) exhibits different forms under different strain rates. Under low strain rate conditions, dislocations tend to pass through GBs and continue to propagate. While under high strain rate conditions, dislocations tend to accumulate at the GBs [50]. In addition, the mechanical characteristics are significantly influenced by the dislocation density. Thirathipviwat et al. [51] investigated the dislocation accumulation and mechanical characteristics of FeNiCoCrMn after cold plastic deformation and concluded that the density of dislocations determines the strength of the mechanical properties.

Besides dislocations, twinning and second phase are common structural defects in solid materials. Twinning is the occurrence of two mirror-symmetric crystal lattice structures in a crystal, which affect the strength and plasticity of HEAs [52]. Several studies have indicated that the mechanical characteristics of HEAs can be enhanced by twinning. Zhang et al. [53] found that maintaining a stable twinning structure during the process of dislocation propagation is the reason why CrCoNi medium-entropy alloys retain their high strength and toughness during mechanical loading. In addition, phase transition cause changes in the crystal structure and lattice defects, thereby affects the strength and plasticity. By controlling the phase transition, it has been demonstrated that HEAs attain exceptional mechanical properties [54]. Li et al. [55] used the MD method to study the strain-induced phase transition (fcc to bcc) in $Co_{25}Ni_{25}Fe_{25}Al_{7.5}Cu_{17.5}$ HEAs. They found that the bcc phase caused a decrease in the material strength while still preserve its exceptional ductility. Moreover, the phase transition was found to be related to the strain rate and crystallographic orientation of the grains. Fang et al. [56] used MD simulations to study the tensile behavior of CoCrFeNiMn dual-phase HEAs. They found that the transformation between FCC and HCP phases had a strong dependence on atomic lattice distortion, which enabled the material to maintain its plasticity. The density of mobile dislocations increased with an increase in strain, enhancing the ductility of the HEAs. Moreover, increase of the density of fixed dislocations enhanced the strength of the HEAs.

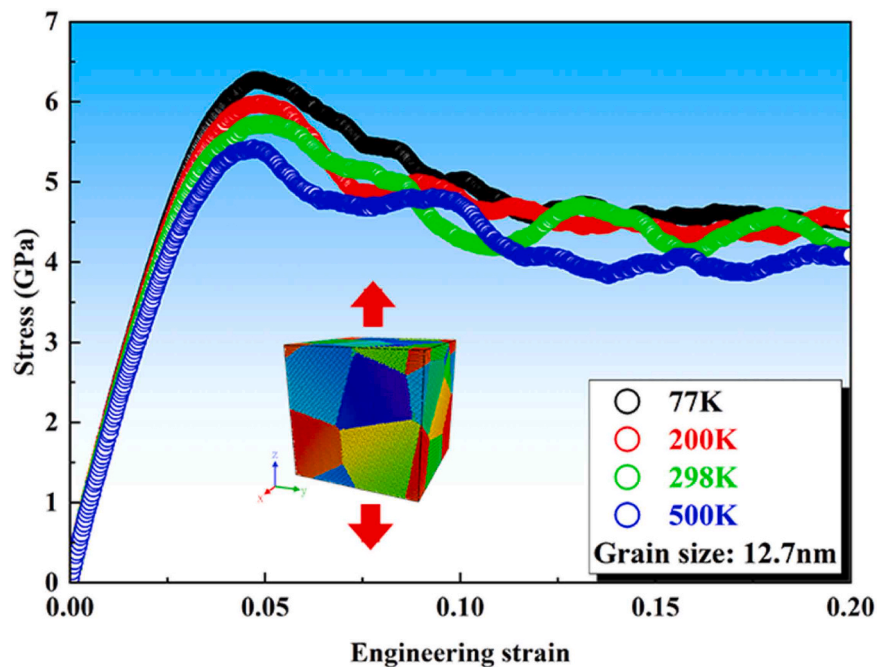The exceptional characteristics of HEAs are impacted by a range of

Fig. 2. CoCrFeNi HEAs with polycrystal structure tensioning processes at various temperatures.The inset in is the polycrystalline model.

elements, including temperature, grain size, dislocation density, twinning, and phase transition. The specific influence mechanism still needs to be further explored. In this work, a combination of experiments and MD simulation is used to analyse the mechanical characteristics of CoCrFeNi HEAs regulated by temperatures and grain size. The nanoscale deformation process in MD simulation can enhance our comprehension of the deformation mechanism of HEAs and provide an important theoretical basis and experimental support for the design and application of HEAs.

2. MD simulation details

The LAMMPS software package was utilized to conduct the MD simulations [57]. Fig. 1 shows a polycrystalline CoCrFeNi HEAs model in FCC phase with an average grain size of 12.7 nm. The average grain size was calculated using the equivalent sphere method, a method also employed in the studies by Pan et al. [33] and Liu et al. [58]. Here, d represents the average grain size (diameter), $V=D^3$ is the cubic simulation box, N is the number of grains within the box, and D stands for the side length of the simulation box.

$$d = \sqrt[3]{\frac{6V/N}{\pi}} = D\sqrt[3]{\frac{6}{\pi N}} = \frac{1.241D}{\sqrt[3]{N}} \tag{1}$$

The construction method is the Voronoi. Use the Atomok tool to fill the simulation box with FCC unit cells, with the positions of the grains and their crystal orientations set in random mode [56,58]. The polycrystalline CoCrFeNi HEAs model consists of 10 grains and a total of 901573 atoms, with dimensions of 22 nm × 22 nm × 22 nm. The atomic quantities of Co, Cr, Fe, and Ni are nearly equal, with values of 225395, 225393, 225391, and 225394, respectively. The lattice constant is a = 0.3615 nm and the time step is 0.001 picoseconds. The periodic boundary conditions were applied to the three orthogonal directions of the simulation box. To mimic a real on-service environment, the model is initially thermodynamically equilibrated with a thermostat targeting the temperature of 300 K for 100 picoseconds. Then the system at five temperatures are prepared by changing the temperature to 500 K, 298 K, 200 K, and 77 K with a temperature change rate of 0.2×10^{12} K/s, followed by full relaxation at a constant temperature for 100 picoseconds. Then, stretching along the Z-axis at a

strain rate of 3×10^9 s^{-1}. The entire simulation process uses the isothermal–isobaric ensemble (NPT), where the temperature and pressure are kept constant during the equilibration stage. Periodic boundary conditions are applied for the three orthogonal directions. Specifically, the pressure is maintained at 0 GPa in all directions. During the stretching stage (along Z direction), the pressure is maintained at 0 GPa in the x and y directions.

3. Results

3.1. Tensile analysis

The strength of CoCrFeNi HEAs exhibits significant temperature dependence, with higher ultimate tensile strength (UTS) at lower temperatures. Our research group has also found similar conclusions in our experimental results [16]. CoCrFeNi have higher strength at low temperatures. At lower temperatures, materials exit the elastic stage later, which suggests that the plasticity of CoCrFeNi HEAs is more difficult to activate. This is because at low temperatures, the ability of atoms and GBs to move is reduced, and plastic deformation usually involves the movement of atoms and dislocations, requiring greater strain to initiate these movements. This also leads to an elevation in the strength of materials at low temperatures. In addition, the various elements in polycrystalline HEAs have different atomic radii and chemical properties. They form solid solutions at different GBs or within grains, which can have a significant impact on the strength and hardness of the crystals [59]. At lower temperatures, the thermal energy of the crystal decreases, leading to greater stability in the solid solution structure, thereby increasing the strength of polycrystalline HEAs. In addition, at higher temperatures, the deformation mechanism of crystals may be dominated by the propagation of internal defects and the slip of dislocations. At lower temperatures, the dominant deformation mechanisms include twinning and transformation-induced plasticity (TRIP) [16, 60–63], and the deformation mechanism of materials at low temperatures is complex and has a significant impact on the strength and toughness of the materials. Fig. 2.
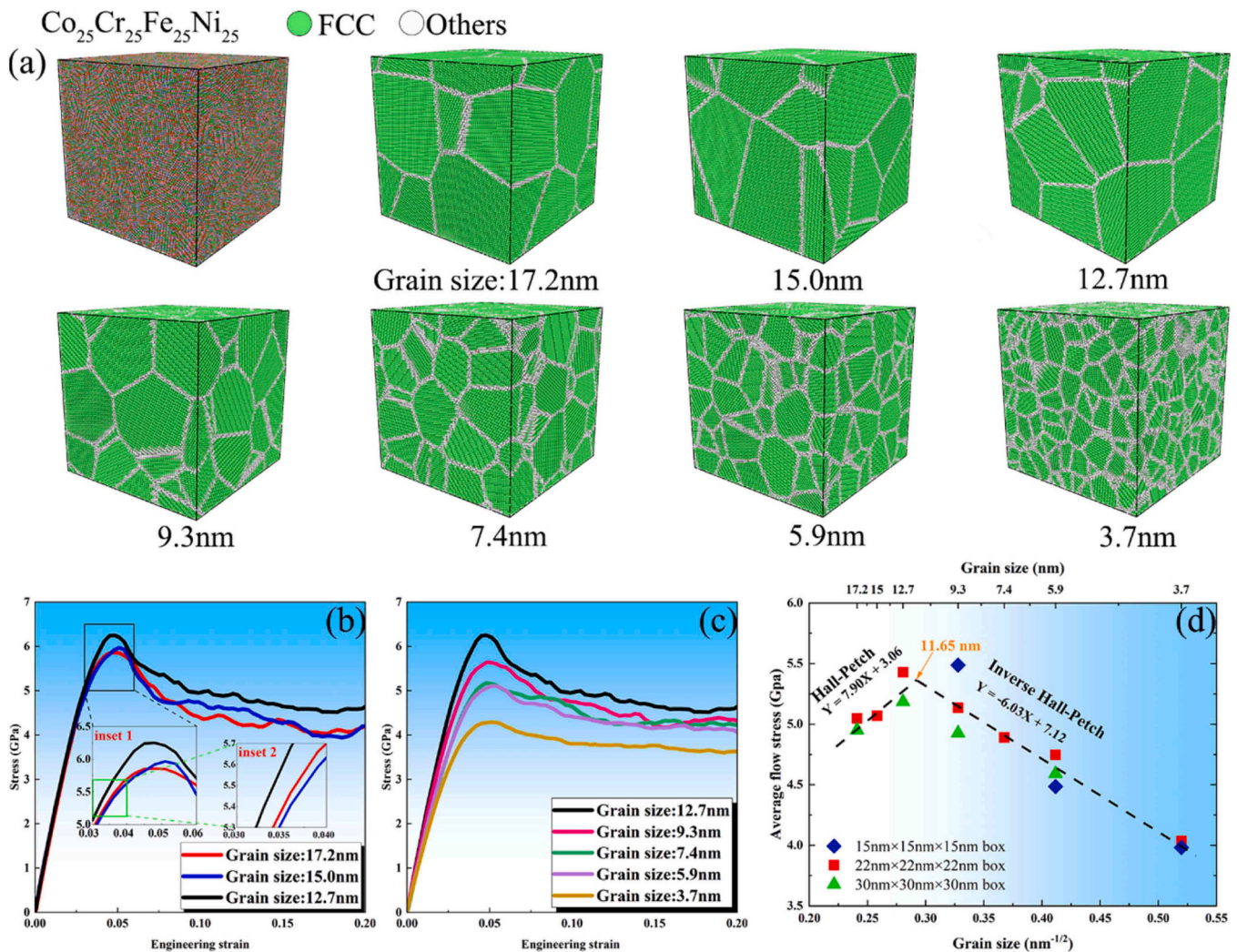
Fig. 3. (a) The 7 models of polycrystalline CoCrFeNi HEAs with various grain sizes (17.2, 15.0, 12.7, 9.3, 7.4, 5.9, and 3.7 nm). The stress-strain curves of the uniaxial tensile tests of the seven systems are displayed in two groups due to the different behaviours: (b) larger grain sizes obeying Hall-Petch effect and (c) smaller grain sizes obeying inverse Hall-Petch effect. The grain size of 12.7 nm is included for both groups for ease of comparison. (d) Average flow stress as a function of the square root of mean grain size ($\sqrt{d}$). Here, we have taken into account the effects resulting from changes in the simulation box size.

3.2. Grain size effect

The influence of grain size on the strength and toughness of CoCr-FeNi HEAs was examined. A strain rate of 3×10^9 s^{-1} and a temperature of 77 K were used during the tensile process. Seven configurations are displayed in Fig. 3(a) for grain size of 17.2, 15.0, 12.7, 9.3, 7.4, 5.9, and 3.7 nm. Fig. 3(b) shows that when the grain size is larger than 12.7 nm, the material strength follows the Hall—Petch relationship that the strength decrease with an increase in grain size. Fig. 3(c) demonstrates that when the grain size is smaller than 12.7 nm, the material strength exhibits the inverse Hall—Petch relationship that the material strength increases with an increase in grain size. Hall [64] found that the presence of grain boundaries in materials forms energy barriers for dislocation propagation. They proposed a relationship between the flow stress in polycrystals σ, the flow stress in single crystals σ_0, and the grain size d in Eq. (2). Petch [65] provided further clarification to Hall findings, stating that the initial dislocations present in a crystal may start to move at stress levels below the yield point but do not extend beyond the grain boundaries. The relationship between flow stress and grain size is expressed by Eq. (3), where K represents the Hall-Petch constant.

$$(\sigma - \sigma_0) \propto d^{-1/2} \tag{2}$$

$$\sigma = \sigma_0 + Kd^{-1/2} \tag{3}$$

In a review by Roberto B et al. [27] on the Hall-Petch effect, it is highlighted that molecular dynamics simulation is one effective method for assessing the Hall-Petch effect. Although the strain rates used in molecular dynamics simulations are relatively high, ranging from 10^8 s^{-1}~10^{12} s^{-1}, no significant impact on the predictive results has been observed due to the differences in strain rates. We have calculated the average flow stress between 5 % and 10 % strain in Fig. 3(d). We considered the potential impact of changes in simulation box size for the same average grain size, by increasing the box size to two different dimensions: 30 nm × 30 nm × 30 nm and 15 nm × 15 nm × 15 nm. For the equiatomic CoCrFeNi HEAs, the critical value of the Hall—Petch effect that we calculated is approximately 11.65 nm. In the study by Pan et al. [33], the critical grain size for the inverse Hall—Petch effect in $Fe_{50}Mn_{30}Co_{10}Cr_{10}$ HEAs was approximately 11.9 nm. In the report by Hu et al. [32], the critical grain size for the Hall—Petch effect in electro-deposited nanocrystalline Ni-Mo was approximately 10 nm. The critical point of the Hall—Petch effect for different materials may vary, but it is in general at the nanometer scale. The storage of dislocations within grains and the accumulation of dislocations at grain boundaries in polycrystalline materials, along with their complex interactions, are
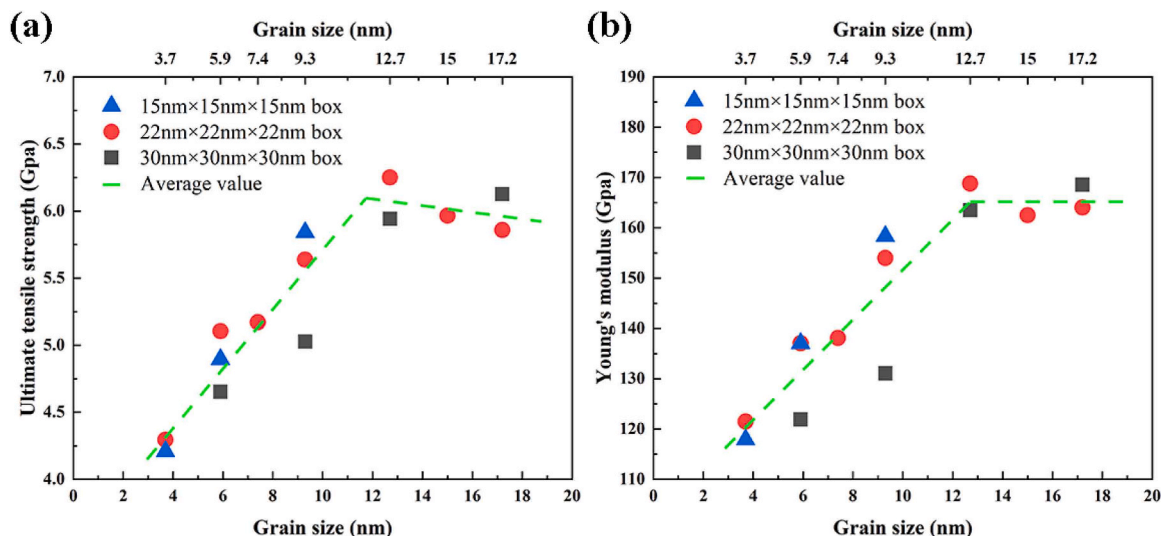
Fig. 4. Changes in the ultimate tensile strength (a) and Young's modulus (b) of CoCrFeNi high-entropy alloy in response to variations in grain size. Three different simulation box sizes are considered.
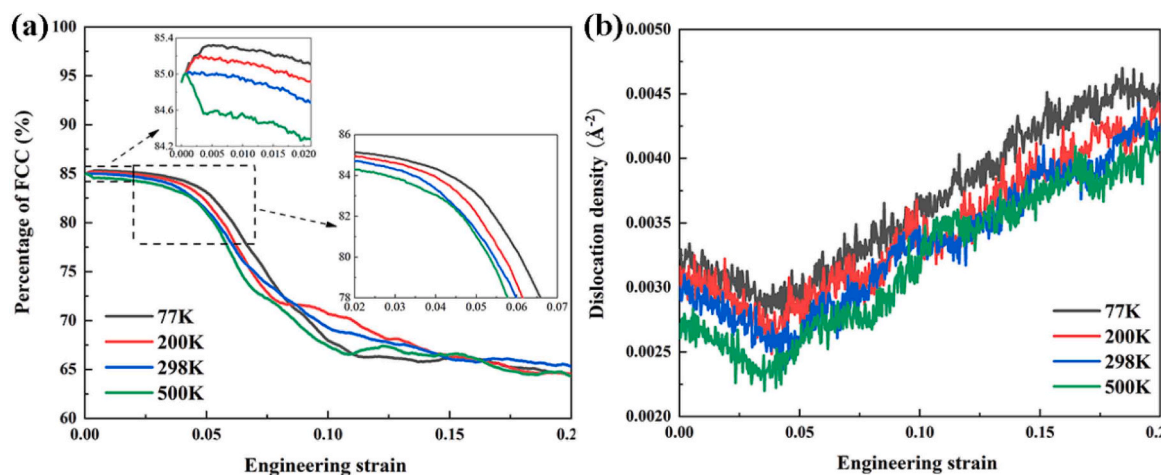

Fig. 5. Percentage of FCC (a) and dislocation density (b) during tensioning at various temperatures.

significant factors contributing to the Hall-Petch effect. The size of the grains significantly influences the capacity for storing dislocations within the grains [28]. A detailed investigation of factors such as grain size, dislocations, and grain boundaries will be conducted in Section 4 of the discussion.

The ultimate tensile strength (UTS) and Young's modulus were analyzed for polycrystalline CoCrFeNi HEAs at different average grain sizes in Fig. 4(a) and Fig. 4(b). Below the critical grain size, both UTS and Young's modulus increase as the grain size increases. However, beyond the critical grain size, this trend is disrupted, and there is a reverse trend, which is consistent with some research results by Pan et al. [33]. Previous studies have shown that during the Hall—Petch regime, as the grain size decreases and the twin spacing decreases, the UTS of the material increases. This is because the number of GBs increases in materials with small GSs, which impedes the movement of dislocations and restricts plastic deformation, thereby increasing the strength of the material. In the inverse Hall—Petch regime, when the grain size is smaller than the critical value, the appearance of a large number of GBs leads to the dominance of internal defects and dislocations, resulting in a decrease in hardness as the grain size decreases [66–68].

4. Discussion

4.1. The influence of dislocation density

In Fig. 2, the polycrystalline CoCrFeNi HEAs exhibits a significant increase in ultimate tensile strength as the temperature decreases, which is related to the high degree of retention of its original crystal phase (FCC) at low temperatures Fig. 5(a) and the higher dislocation density Fig. 5(b). This is due to the fact that atoms exhibit weaker thermal vibrations at low temperatures, indicating a lower average kinetic energy for atoms at low temperatures. As a result, it becomes more challenging for atoms to overcome the existing lattice barriers, making the FCC crystal phase less prone to transitioning into other phases. In Fig. 5(b), as the temperature decreases, the CoCrFeNi HEAs exhibits higher dislocation density. This is because dislocations are defects within the crystal and can be seen as irregularities in the arrangement of atoms within the lattice. At low temperatures, the movement of dislocations is restricted due to the reduced thermal vibrations of atoms, making it more challenging for dislocations to traverse the crystal lattice and to be absorbed by grain boundaries, as illustrated in the propagation process of SFs dislocations in Fig. 9. This results in dislocations lingering within the crystal for longer periods, gradually accumulating and ultimately
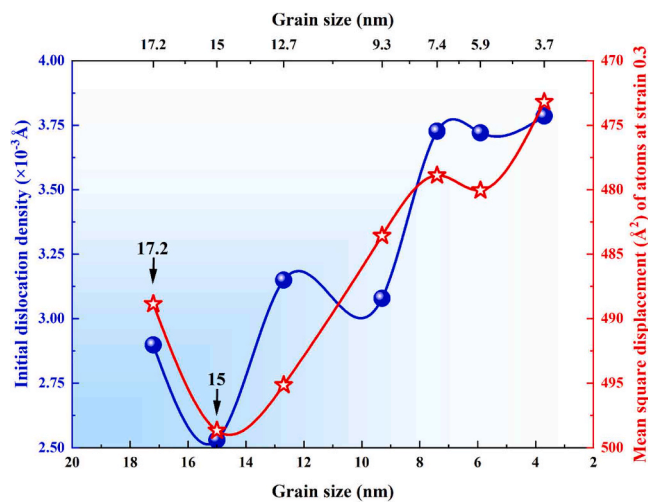
Fig. 6. Statistics of initial dislocation density (left Y axis) and mean square displacement of atoms at strain 0.3 (right Y axis) for CoCrFeNi HEAs with seven different grain sizes. The left Y-axis scale increases from bottom to top, while the right Y-axis scale decreases from bottom to top.

increasing the dislocation density.

Fig. 6 presents a statistical analysis of the initial dislocation density and MSD of atoms of CoCrFeNi HEAs with seven different GSs. Calculation was performed using OVITO [69]. The reduction of grain size generally leads to an increase in the overall dislocation density within the material, particularly at grain boundaries in Fig. 8(c). The elevation of dislocation density, including line and planar dislocations, significantly affects the atomic motion during the process of tensile deformation. The presence of dislocations can impede atomic motion processes, resulting in changes in the tensile strength and elongation of materials.

MSD is the most common measure in the spatial range of random motion [70,71]. In Fig. 6, there is a strong correlation between the magnitude of atomic displacement (represented by MSD) during tensile deformation and the initial dislocation density of the model. The increase in dislocation density noticeably slows down the atomic motion during the tensioning process, leading to a decrease in the MSD value (please note that the scale on the right Y-axis decreases from bottom to top). By observing the x-axis and the left y-axis, the density of initial dislocations shows an upwards trend as the grain size decreases. However, due to the randomness of the model, the curve did not show a strictly monotonic increase. For example, the dislocation density of the sample with a grain size of 17.2 nm was actually higher than that of the sample with a grain size of 15 nm. In the inset 2 of Fig. 3(b), the strength of the 17.2 nm grain size sample is greater than that of the 15 nm grain size sample in the early to mid-elastic stage, which is consistent with the higher dislocation density results. While the sample with a grain size of 15 nm has a higher UTS than the sample with a grain size of 17.2 nm, which could be attributed to other factors such as twin strengthening and variations in the dislocation storage capacity within individual grains (Fig. 8). Fig. 7 shows the internal structural changes of a single grain during the tensile process, including the origin and evolution of dislocations, as well as the generation and propagation of SFs. During the tensioning process, Shockley dislocations are mainly dominant, and dislocations generally originate at GBs (Fig. 7(a)). Dislocations of different angles may interact with each other and produce Stair-Rod dislocations (Fig. 7(d)) [72]. Fig. 7(e-h) show the propagation process of SFs within a single grain, and different SFs may experience blocking effects during their propagation.

To further investigate the phenomena of "smaller is stronger" and "smaller is weaker" in relation to material strength due to a reduction in grain size, an analysis was conducted on the dislocations stored within single grains, including both line and planar dislocations, as well as the presence of line dislocations at grain boundaries. In Fig. 8(a) and (b), as the grain size decreases, the density of line dislocations stored within
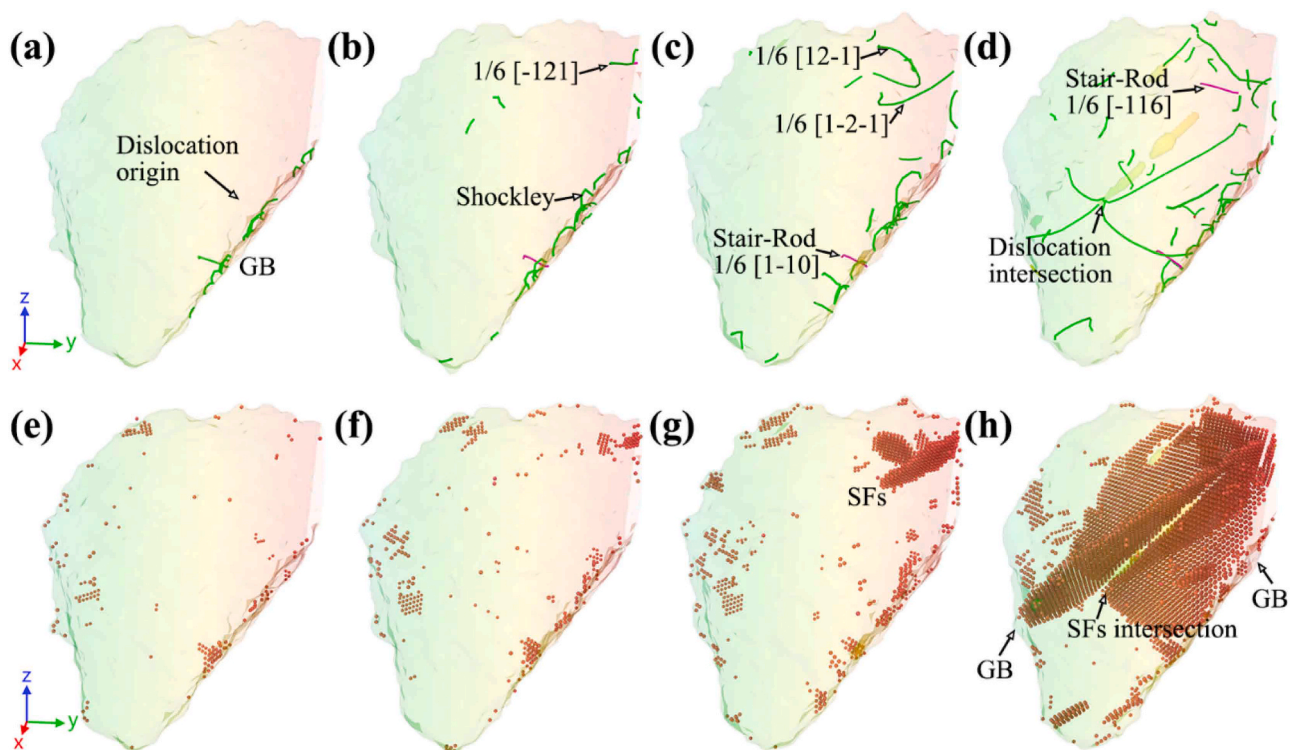

Fig. 7. The microstructural evolution of a single grain with a grain size of 12.7 nm during tensile deformation at 77 K. To facilitate observation, (a-d) show only dislocation lines without atoms, while (e-h) show only HCP atoms without FCC atoms and dislocation lines. The color of the grains is configured based on their coordinate positions. Strain: (a) and (e) 4 %, (b) and (f) 5 %, (c) and (g) 6 %, and (d) and (h) 8 %.
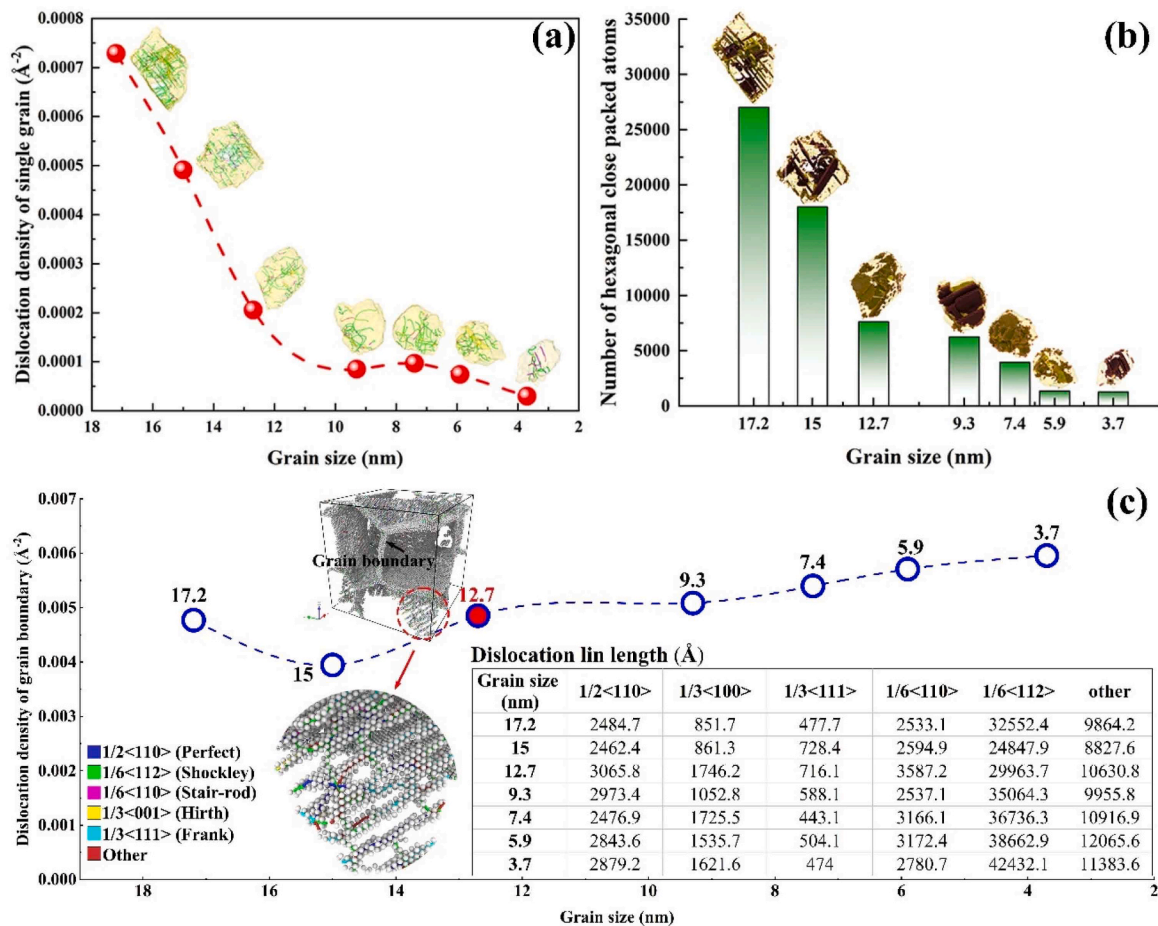
Fig. 8. Dislocation lines (a) and stacking faults (b) stored in single grain of different sizes, dislocation line density at grain boundaries (c).

The dislocation line length table within Fig. 8(c):

Grain size (nm)	1/2<110>	1/3<100>	1/3<111>	1/6<110>	1/6<112>	other
17.2	2484.7	851.7	477.7	2533.1	32552.4	9864.2
15	2462.4	861.3	728.4	2594.9	24847.9	8827.6
12.7	3065.8	1746.2	716.1	3587.2	29963.7	10630.8
9.3	2973.4	1052.8	588.1	2537.1	35064.3	9955.8
7.4	2476.9	1725.5	443.1	3166.1	36736.3	10916.9
5.9	2843.6	1535.7	504.1	3172.4	38662.9	12065.6
3.7	2879.2	1621.6	474	2780.7	42432.1	11383.6

individual grains and the number of SFs exhibit a decreasing trend. In Fig. 8(c), the density of line dislocations at grain boundaries shows an increasing trend with a reduction in grain size. The coordinated interaction between the dislocation density within grains and at grain boundaries primarily governs the changes in material strength as the grain size decreases. With a reduction in grain size, the number of grains in contact with a single grain at any given moment increases. Due to the different grain orientations, this increase in the number of grain boundaries leads to an elevation in the density of dislocations at grain boundaries. In Fig. 8(a) and (c), the density of dislocations at grain boundaries is much higher than that within the grains. The grain boundaries serve as effective energy barriers for atomic motion within the crystal and the propagation of SFs, thereby coordinating the dynamic changes in material strength. Indeed, within individual grains, there is also a subgrain size variation that occurs during material elongation. In Fig. 8(b), SFs are present within individual grains. The formation of SFs can influence the grain orientation within the individual grain, leading to the formation of two or more subgrains. A detailed analysis of this phenomenon is further discussed in Section 4.2. Due to the disordered nature of atoms at grain boundaries, they are generally considered as defects. It is undeniable that the presence of a moderate amount of dislocations can enhance the strength and even the toughness of a material. However, as the grain size decreases, the storage capacity of dislocations within the grains decreases, resulting in the accumulation of more dislocations at grain boundaries and the generation of numerous defects. This inevitably leads to a decrease in material strength.

4.2. The influence of twinning and phase transformation

Fig. 9 shows the structural changes of CoCrFeNi HEAs with an average grain size of 12.7 during uniaxial tension at a strain rate of $3 \times 10^9 s^{-1}$. SFs (red structures in Fig. 9) usually originate at GBs. As the tensioning process progresses, the movement forms of SFs mainly include the following: SFs propagate in the crystal, SFs are absorbed when propagating to the grain boundary, SFs encounter obstruction from other SFs during propagation, and intrinsic stacking faults (ISFs) transform into extrinsic stacking faults (ESFs) in Fig. 10(a). During these processes, SFs propagation may cause lattice distortion, leading to cracks and fracture, which can have a negative impact on the strength and toughness of the material. The absorption of SFs by GBs may prevent the propagation of dislocations. Additionally, the hindrance of SF propagation between SFs enlarges the strength of materials. At lower temperatures, the propagation rate of SFs slows down, increasing the probability of SFs being blocked, thereby enhancing the strength the material. Conversely, at high temperatures, the propagation rate of SFs increases, and the strength of the material may decrease. Ding et al. [73] found that the TWIP and TRIP mechanisms in CrCoNi alloys are prone to form thin high-density twin boundaries during plastic deformation. It was noted that the formation of dislocation slip, twinning, and SFs occurred in sequence, dominating the plastic deformation process.

The transformation between the ISF and ESF occurs during the straining process of CoCrFeNi HEAs (Fig. 10). Twinning can result from the propagation of SFs, and the formation of large-scale SFs can cause a transition from the FCC to HCP phase, indicating that the TWIP effect and TRIP effect occursequentially during the material straining process. Popagation of SFs within individual grains can lead to the formation of

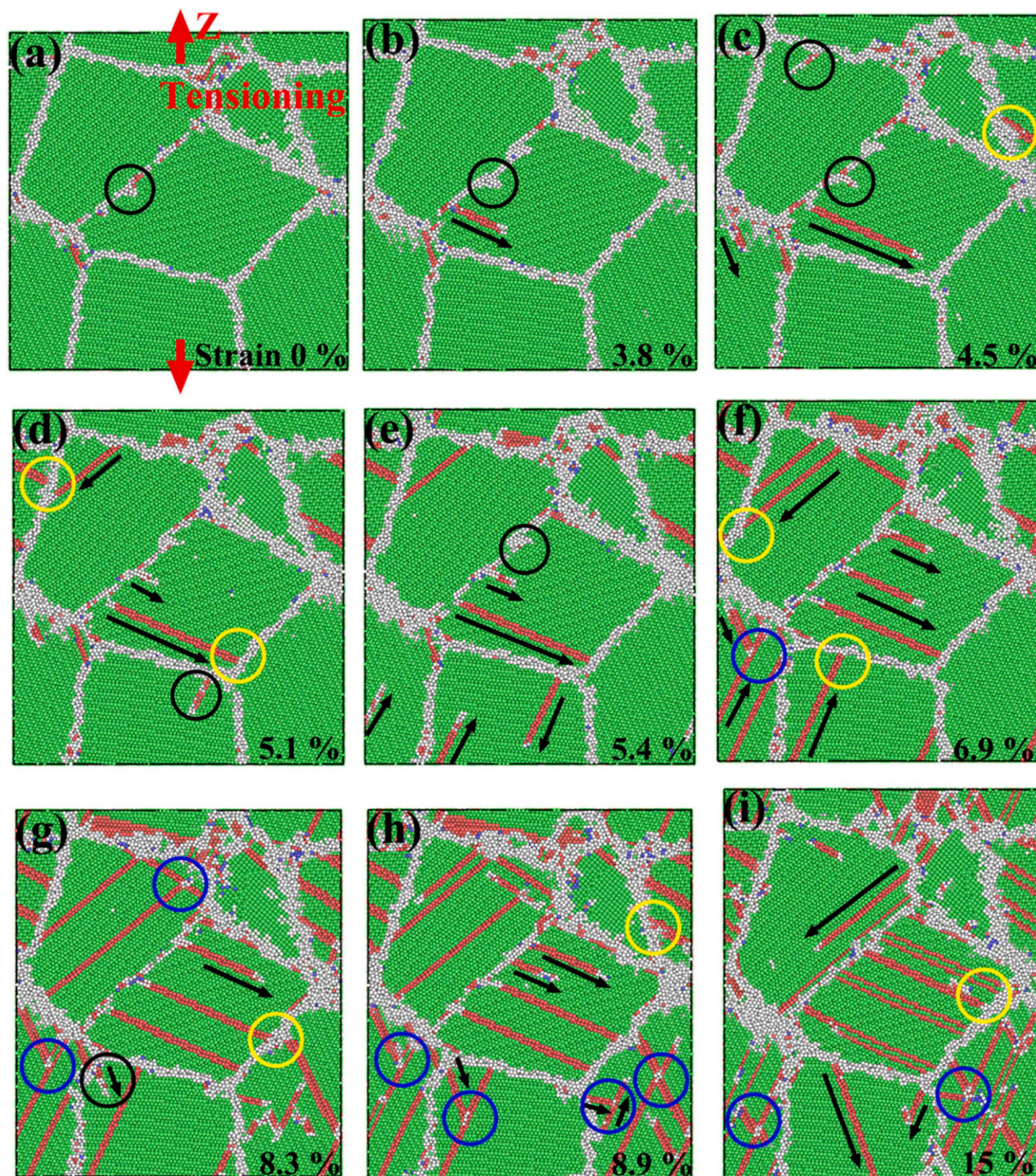**Fig. 9.** Morphology changes of CoCrFeNi HEAs with a grain size of 12.7 nm during the tensile process. Green: fcc, red: hcp, blue: bcc, white: GBs. The black circle and arrow represent the origin and spread of SFs, the yellow circle represents SFs being absorbed by GBs, and the blue circle represents the spread of SFs being blocked by other SFs. The strains applied in the z direction in (a-i) are 0 %, 3.8 %, 4.5 %, 5.1 %, 5.4 %, 6.9 %, 8.3 %, 8.9 %, and 15 %, respectively.

subgrains, resulting in the occurrence of the dynamic Hall-Petch effect, which affects the strength and toughness of the material. Some studies report that the SF energy of CoCrNi-based HEAs is negative at low temperatures [74], and the formation of inherent SFs may be a spontaneous process. In transferable FCC alloys, twinning is the main deformation mode [75], which enhances the ductility of HEAs. The Hall—Petch effect is improved by strengthening the fractured grains, which improves the strength of materials.

5. Conclusions

We have investigated the grain size and temperature effect on the mechanical properties of polycrystalline CoCrFeNi HEAs using molecular dynamics simulation methods. The critical point of the inverse Hall-Petch effect appears around an average grain size of 11.65 nm. Dislocation density plays a dominant role in the tensile strength of CoCrFeNi HEAs, with higher dislocation density typically reducing the atomic motion. The storage capacity of dislocations within grains decreases as grain size decreases, leading to the accumulation of more dislocations at grain boundaries, resulting in defects. When defects within the material dominate, the inverse Hall-Petch effect occurs. The mechanical properties of polycrystalline CoCrFeNi HEAs are significantly influenced by temperature. At lower temperatures, CoCrFeNi HEAs exhibit higher tensile strength due to the underlying reason of weakened atomic thermal vibrations. The reduced atomic thermal vibrations result in the slowing down of dislocation motion within the crystal, a closer interatomic spacing, and a moderate increase in dislocation density, ultimately leading to the improvement in material tensile strength.
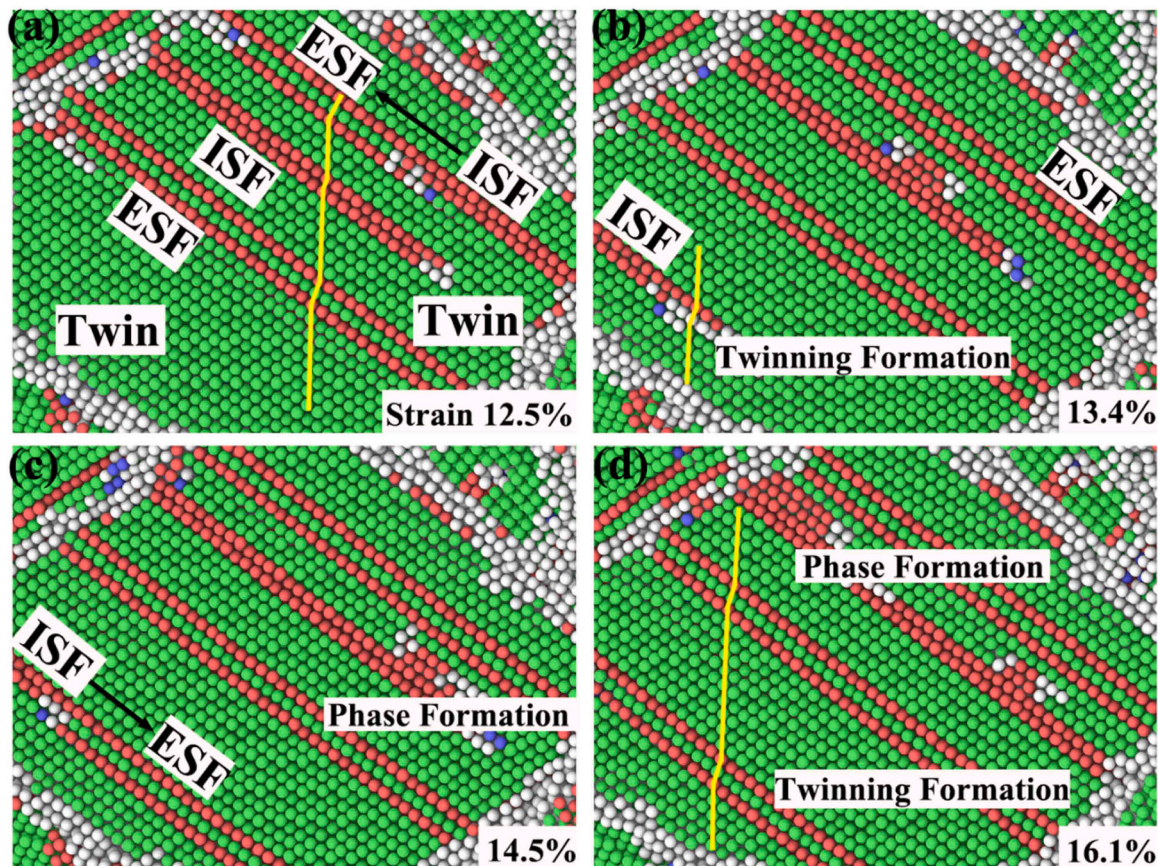
Fig. 10. The deformation mechanism of CoCrFeNi HEAs with an average grain size of 12.7 nm during tensile deformation includes transformation of ISF and ESF, formation of twins, and PT (FCC to HCP). The strains applied in (a-d) are 12.5 %, 13.4 %, 14.5 %, and 16.1 %, respectively.

Our atomistic insights into the mechanical properties of polycrystalline CoCrFeNi HEAs may provide some support for the development of future superior HEAs.

CRediT authorship contribution statement

Lu Xie: Conceptualization, Funding acquisition, Methodology, Project administration, Resources, Supervision, Writing – original draft, Writing – review & editing. **Guangda Wu:** Data curation, Formal analysis, Methodology, Validation, Writing – original draft, Writing – review & editing. **Qing Peng:** Funding acquisition, Project administration, Software, Writing – original draft. **Junpeng Liu** : Methodology, Investigation, Resources. **Dongyue Li:** Writing – review & editing, Validation. **Wenrui Wang:** Funding acquisition, Supervision, Methodology, Project administration.

Declaration of Competing Interest

The work described has not been submitted elsewhere for publication, and all the authors listed have approved the manuscript that is enclosed. We have no conflicts of interest to disclose.

Data availability

Data will be made available on request.

Acknowledgement

Appendix A. Supporting information

References

[1] R.S. Mishra, R.S. Haridas, P. Agrawal, High entropy alloys – Tunability of deformation mechanisms through integration of compositional and microstructural domains, Mater. Sci. Eng. A, Struct. Mater.: Prop., Microstruct. Process. 812 (2021), 141085.

[2] Y. Tang, R. Wang, B. Xiao, Z. Zhang, S. Li, J. Qiao, S. Bai, Y. Zhang, P.K. Liaw, A review on the dynamic-mechanical behaviors of high-entropy alloys, Prog. Mater. Sci. 135 (2023), 101090.

[3] P.G. Easo, D. Raabe, O.R. Robert, High-entropy alloys, Nat. Rev. Mater. 4 (2019) 515.

[4] Y. Zhang, T.T. Zuo, Z. Tang, M.C. Gao, K.A. Dahmen, P.K. Liaw, Z.P. Lu, Microstructures and properties of high-entropy alloys, Prog. Mater. Sci. 61 (2014) 1.

[5] W. Wang, J. Wang, H. Yi, W. Qi, Q. Peng, Effect of molybdenum additives on corrosion behavior of (CoCrFeNi)100−xMox high-entropy alloys, Entropy-Switz 20 (2018) 908.

[6] Y. Li, R. Li, Q. Peng, Enhanced surface bombardment resistance of the CoNiCrFeMn high entropy alloy under extreme irradiation flux, Nanotechnology 31 (2020) 25703.

[7] C. Lu, T. Yang, K. Jin, G. Velisa, P. Xiu, M. Song, Q. Peng, F. Gao, Y. Zhang, H. Bei, W.J. Weber, L. Wang, Oak Ridge National Lab. ORNL ORTU, Energy FRCE. Enhanced void swelling in NiCoFeCrPd high-entropy alloy by indentation-induced dislocations, Mater. Res. Lett. 6 (2018) 584.

[8] T. Shi, S. Lyu, Z. Su, Y. Wang, X. Qiu, D. Sun, Y. Xin, W. Li, J. Cao, Q. Peng, Y. Li, C. Lu, Spatial inhomogeneity of point defect properties in refractory multi-principal element alloy with short-range order: a first-principles study, J. Appl. Phys. 133 (2023) 75103.

[9] T. Shi, X. Qiu, Y. Zhou, S. Lyu, J. Li, D. Sun, Q. Peng, Y. Xin, C. Lu, Unconventional energetics of small vacancy clusters in BCC high-entropy alloy Nb0.75ZrTiV0.5, J. Mater. Sci. Technol. 146 (61) (2023).

[10] W. Zhang, P.K. Liaw, Y. Zhang, Science and technology in high-entropy alloys, Sci. China Mater. 61 (2018) 2.

[11] Y. Li, J. Du, P. Yu, R. Li, S. Shinzato, Q. Peng, S. Ogata, Chemical ordering effect on the radiation resistance of a CoNiCrFeMn high-entropy alloy, Comp. Mater. Sci. 214 (2022), 111764.

[12] C. Lu, T. Yang, K. Jin, G. Velisa, P. Xiu, Q. Peng, F. Gao, Y. Zhang, H. Bei, W. J. Weber, L. Wang, Irradiation effects of medium-entropy alloy NiCoCr with and without pre-indentation, J. Nucl. Mater. 524 (2019) 60.

[13] Z.H. Sun, J. Zhang, G.X. Xin, L. Xie, L.C. Yang, Q. Peng, Tensile mechanical properties of CoCrFeNiTiAl high entropy alloy via molecular dynamics simulations, Intermetallics 142 (2022), 107444.

[14] D. Liu, Q. Yu, S. Kabra, M. Jiang, P. Forna-Kreutzer, R. Zhang, M. Payne, F. Walsh, B. Gludovatz, M. Asta, A.M. Minor, E.P. George, R.O. Ritchie, Exceptional fracture toughness of CrCoNi-based medium- and high-entropy alloys at 20 kelvin, Science (Am. Assoc. Adv. Sci.) 378 (2022) 978.

[15] D. Li, Y. Zhang, The ultrahigh charpy impact toughness of forged AlxCoCrFeNi high entropy alloys at room and cryogenic temperatures, Intermetallics 70 (2016) 24.

[16] J. Liu, X. Guo, Q. Lin, Z. He, X. An, L. Li, P.K. Liaw, X. Liao, L. Yu, J. Lin, L. Xie, J. Ren, Y. Zhang, Excellent ductility and serration feature of metastable CoCrFeNi high-entropy alloy at extremely low temperatures, Sci. China Mater. 62 (2019) 853.

[17] D. Li, C. Li, T. Feng, Y. Zhang, G. Sha, J.J. Lewandowski, P.K. Liaw, Y. Zhang, High-entropy Al0.3CoCrFeNi alloy fibers with high tensile strength and ductility at ambient and cryogenic temperatures, Acta Mater. 123 (285) (2017).

[18] F. Otto, A. Dlouhý, C. Somsen, H. Bei, G. Eggeler, E.P. George, The influences of temperature and microstructure on the tensile properties of a CoCrFeMnNi high-entropy alloy, Acta Mater. 61 (2013) 5743.

[19] Z. Li, S. Zhao, R.O. Ritchie, M.A. Meyers, Mechanical properties of high-entropy alloys with emphasis on face-centered cubic alloys, Prog. Mater. Sci. 102 (2019) 296.

[20] Y. Qi, H. Xu, T. He, M. Feng, Effect of crystallographic orientation on mechanical properties of single-crystal CoCrFeMnNi high-entropy alloy, Mater. Sci. Eng.: A 814 (2021), 141196.

[21] P. Cao, Maximum strength and dislocation patterning in multi–principal element alloys, Sci. Adv. 8 (2022) q7433.

[22] Y. Tian, S. Peng, S. Chen, Z. Gu, Y. Yang, X. Shang, G. Deng, L. Su, S. Sun, Temperature-dependent tensile properties of ultrafine-grained C-doped CoCrFeMnNi high-entropy alloy, Rare Met. 41 (2022) 2877.

[23] T. Zhang, R.D. Zhao, F.F. Wu, S.B. Lin, S.S. Jiang, Y.J. Huang, S.H. Chen, J. Eckert, Transformation-enhanced strength and ductility in a FeCoCrNiMn dual phase high-entropy alloy, Mater. Sci. Eng.: A 780 (2020) 139182.

[24] S.T. Abraham, S.S. Bhat, Crystal plasticity finite element modelling on the influence of grain size and shape parameters on the tensile stiffness and yield strength, Mater. Sci. Eng.: A 877 (2023), 145155.

[25] J. Yuan, M. Huang, Y. Li, L. Wang, H. Li, W. Xu, Revealing the grain size-dependent twinning variants and the associated strengthening mechanisms in a carbon-free austenitic steel, Mater. Sci. Eng.: A 864 (2023), 144577.

[26] N J P, Metallurgy at Leeds: Prof, Nature (1956) 178.

[27] R.B. Figueiredo, M. Kawasaki, T.G. Langdon, Seventy years of Hall-Petch, ninety years of superplasticity and a generalized approach to the effect of grain size on flow stress, Prog. Mater. Sci. 137 (2023), 101131.

[28] Q. Han, X. Yi, A unified mechanistic model for Hall–Petch and inverse Hall–Petch relations of nanocrystalline metals based on intragranular dislocation storage, J. Mech. Phys. Solids 154 (2021), 104530.

[29] T. Fang, C. Huang, T. Chiang, Effects of grain size and temperature on mechanical response of nanocrystalline copper, Mater. Sci. Eng.: A 671 (2016) 1.

[30] D.J. Lloyd, S.A. Court, Influence of grain size on tensile properties of Al-Mg alloys, Mater. Sci. Technol.-Lond. 19 (2013) 1349.

[31] R. Zheng, J. Du, S. Gao, H. Somekawa, S. Ogata, N. Tsuji, Transition of dominant deformation mode in bulk polycrystalline pure Mg by ultra-grain refinement down to sub-micrometer, Acta Mater. 198 (2020) 35.

[32] J. Hu, Y.N. Shi, X. Sauvage, G. Sha, K. Lu, Grain boundary stability governs hardening and softening in extremely fine nanograined metals, Science 355 (2017) 1292.

[33] Z. Pan, Y. Fu, Y. Wei, X. Yan, H. Luo, X. Li, Deformation mechanisms of TRIP–TWIP medium-entropy alloys via molecular dynamics simulations, Int. J. Mech. Sci. 219 (2022), 107098.

[34] S.S.R. Pulagam, A. Dutta, Limitations of meta-atom potential for analyzing dislocation core structure in TWIP steel, Mech. Mater. 178 (2023), 104563.

[35] A. Jarlöv, W. Ji, Z. Zhu, Y. Tian, R. Babicheva, R. An, H.L. Seet, M.L.S. Nai, K. Zhou, Molecular dynamics study on the strengthening mechanisms of Cr–Fe–Co–Ni high-entropy alloys based on the generalized stacking fault energy, J. Alloy Compd. 905 (2022), 164137.

[36] M. Bahramyan, R.T. Mousavian, J.G. Carton, D. Brabazon, Nano-scale simulation of directional solidification in TWIP stainless steels: a focus on plastic deformation mechanisms, Mater. Sci. Eng.: A 812 (2021), 140999.

[37] M. Bahramyan, R.T. Mousavian, D. Brabazon, Study of the plastic deformation mechanism of TRIP–TWIP high entropy alloys at the atomic level, Int. J. Plasticity 127 (2020), 102649.

[38] R. Mohammadzadeh, Deformation characteristics of nanocrystalline TWIP steel under uniaxial tension and compression, Mech. Mater. 138 (2019), 103147.

[39] R. Mohammadzadeh, M. Mohammadzadeh, Inverse grain size effect on twinning in nanocrystalline TWIP steel, Mater. Sci. Eng.: A 747 (2019) 265.

[40] R. Mohammadzadeh, Reversible deformation in nanocrystalline TWIP steel during cyclic loading by partial slip reversal and detwinning, Mater. Sci. Eng.: A 782 (2020), 139251.

[41] Q. Peng, F. Meng, Y. Yang, C. Lu, H. Deng, L. Wang, S. De, F. Gao, Shockwave generates < 100 > dislocation loops in bcc iron, Nat. Commun. (2018) 9.

[42] S.H. Joo, H. Kato, M.J. Jang, J. Moon, C.W. Tsai, J.W. Yeh, H.S. Kim, Tensile deformation behavior and deformation twinning of an equimolar CoCrFeMnNi high-entropy alloy, Mater. Sci. Eng.: A 689 (2017) 122.

[43] T. Shi, Z. Su, J. Li, C. Liu, J. Yang, X. He, D. Yun, Q. Peng, C. Lu, Distinct point defect behaviours in body-centered cubic medium-entropy alloy NbZrTi induced by severe lattice distortion, Acta Mater. 229 (2022), 117806.

[44] L. Qian, H. Bao, R. Li, Q. Peng, Atomistic insights of a chemical complexity effect on the irradiation resistance of high entropy alloys, Materials Advances 3 (2022) 1680–1686.

[45] Y. Liu, R. Li, Q. Peng, The preexisting edge dislocations as recombination center of point defects enhancing irradiation tolerance in CoCrCuFeNi high entropy alloy, Materialia 21 (2022), 101307.

[46] M. Chen, D. Xie, N. Li, M.A. Zikry, Dislocation-density evolution and pileups in bicrystalline systems, Mater. Sci. Eng.: A 870 (2023), 144812.

[47] J. Li, Q. Fang, B. Liu, Y. Liu, Y. Liu, Atomic-scale analysis of nanoindentation behavior of high-entropy alloy, J. Micromech. Mol. Phys. 01 (2016) 1650001.

[48] D. Doan, Effects of crystal orientation and twin boundary distance on mechanical properties of FeNiCrCoCu high-entropy alloy under nanoindentation, Mater. Chem. Phys. 291 (2022), 126725.

[49] H. Pan, Y. He, X. Zhang, Interactions between Dislocations and boundaries during deformation, Materials 14 (2021) 1012.

[50] N.V. Malyar, G. Dehm, C. Kirchlechner, Strain rate dependence of the slip transfer through a penetrable high angle grain boundary in copper, Scr. Mater. 138 (2017) 88.

[51] P. Thirathipviwat, G. Song, J. Bednarcik, U. Kühn, T. Gemming, K. Nielsch, J. Han, Compositional complexity dependence of dislocation density and mechanical properties in high entropy alloy systems, Prog. Nat. Sci.: Mater. Int. 30 (2020) 545.

[52] Z. Lyu, X. Fan, C. Lee, S. Wang, R. Feng, P.K. Liaw, Fundamental understanding of mechanical behavior of high-entropy alloys at low temperatures: a review, J. Mater. Res. 33 (2018) 2998.

[53] Z. Zhang, H. Sheng, Z. Wang, B. Gludovatz, Z. Zhang, E.P. George, Q. Yu, S.X. Mao, R.O. Ritchie, Dislocation mechanisms and 3D twin architectures generate exceptional strength-ductility-toughness combination in CrCoNi medium-entropy alloy, Nat. Commun. (2017) 8.

[54] J. Cao, J. Jin, S. Li, M. Wang, S. Tang, Q. Peng, Y. Zong, Effect of microstructure on the onset strain and rate per strain of deformation-induced martensite transformation in Q&P steel by modeling, Materials 15 (2022) 952.

[55] J. Li, Q. Fang, B. Liu, Y. Liu, Transformation induced softening and plasticity in high entropy alloys, Acta Mater. 147 (2018) 35.

[56] Q. Fang, Y. Chen, J. Li, C. Jiang, B. Liu, Y. Liu, P.K. Liaw, Probing the phase transformation and dislocation evolution in dual-phase high-entropy alloys, Int. J. Plasticity 114 (2019) 161.

[57] A.P. Thompson, H.M. Aktulga, R. Berger, D.S. Bolintineanu, W.M. Brown, P. S. Crozier, In T Veld PJ, Kohlmeyer A, Moore SG, Nguyen TD, Shan R, Stevens MJ, Tranchida J, Trott C, Plimpton SJ. LAMMPS - a flexible simulation tool for particle-based materials modeling at the atomic, meso, and continuum scales, Comput. Phys. Commun. 271 (2022), 108171.

[58] P. Hirel, Atomsk: A tool for manipulating and converting atomic data files, Comput. Phys. Commun. 197 (2015) 212.

[59] H.W. Yao, J.W. Qiao, J.A. Hawk, H.F. Zhou, M.W. Chen, M.C. Gao, Mechanical properties of refractory high-entropy alloys: experiments and modeling, J. Alloy Compd. 696 (2017) 1139.

[60] X. Zhang, X. Lu, J. Zhao, Q. Kan, Z. Li, G. Kang, Temperature effect on tensile behavior of an interstitial high entropy alloy: crystal plasticity modeling, Int. J. Plasticity 150 (2022) 103201.

[61] Z. Wang, W. Lu, D. Raabe, Z. Li, On the mechanism of extraordinary strain hardening in an interstitial high-entropy alloy under cryogenic conditions, J. Alloy Compd. 781 (2019) 734.

[62] Z. Li, C.C. Tasan, H. Springer, B. Gault, D. Raabe, Interstitial atoms enable joint twinning and transformation induced plasticity in strong and ductile high-entropy alloys, Sci. Rep.-UK (2017) 7.

[63] D. Li, Z. Li, L. Xie, Y. Zhang, W. Wang, Cryogenic mechanical behavior of a TRIP-assisted dual-phase high-entropy alloy, Nano Res. 15 (2022) 4859.

[64] E O H, The deformation and ageing of mild steel: III discussion of results, Proc. Phys. Soc. Sect. B 64 (1951) 747.

[65] N J P, The cleavage strength of polycrystals, J. Iron Steel Inst. 174 (1953) 25.

[66] C. Suryanarayana, D. Mukhopadhyay, S.N. Patankar, F.H. Froes, Grain size effects in nanocrystalline materials, Hall-petch relation in nanocrystalline solids 7 (1992) 2144.

[67] T.G. Nieh, J. Wadsworth, Hall-petch relation in nanocrystalline solids, Scr. Metall. Mater. 25 (1991) 955.

[68] V.G. Gryaznov, V.A. Solov'Ev, L.I. Trusov, The peculiarities of initial stages of deformation in nanocrystalline materials (NCMs), Scr. Metall. Mater. 24 (1990) 1529.

[69] A. Stukowski, Visualization and analysis of atomistic simulation data with OVITO–the open visualization tool, Model Simul. Mater. Sci. 18 (2010) 15012.

[70] Z. Sun, B. Liu, C. He, L. Xie, Q. Peng, Shift of creep mechanism in nanocrystalline NiAl alloy, Materials 12 (2019) 2508.

[71] Q. Qin, W. He, L. Xie, J. Deng, X. Zhu, Q. Peng, Nonlinear diffusion, bonding, and mechanics of the interface between austenitic steel and iron, Phys. Chem. Chem. Phys. 21 (2019) 1464.

[72] R. Liu, J. Tang, J. Jiang, X. Li, Y. Wei, Stacking fault induced hardening and grain size effect in nanocrystalline CoNiCrFeMn high-entropy alloy, Extreme Mech. Lett. 56 (2022), 101875.

[73] L. Ding, A. Hilhorst, H. Idrissi, P.J. Jacques, Potential TRIP/TWIP coupled effects in equiatomic CrCoNi medium-entropy alloy, Acta Mater. 234 (2022), 118049.

[74] Y.H. Zhang, Y. Zhuang, A. Hu, J.J. Kai, C.T. Liu, The origin of negative stacking fault energies and nano-twin formation in face-centered cubic high entropy alloys, Scr. Mater. 130 (2017) 96.

[75] S. Huang, H. Huang, W. Li, D. Kim, S. Lu, X. Li, E. Holmström, S.K. Kwon, L. Vitos, Twinning in metastable high-entropy alloys, Nat. Commun. (2018) 9.